Available online at www.sciencedirect.com
SCIENCE DIRECT®
Journal of Sound and Vibration 275 (2004) 893–915
JOURNAL OF SOUND AND VIBRATION
www.elsevier.com/locate/jsvi

A study of the weak shock wave propagating through an engine exhaust silencer system

H.-D. Kim[a,*], Y.-H. Kweon[a], T. Setoguchi[b]

[a] School of Mechanical Engineering, Andong National University, 388, Songchun-dong, Andong 760-749, South Korea
[b] Department of Mechanical Engineering, Saga University, 1, Honjo, Saga 840-8502, Japan

Received 2 May 2002; accepted 14 July 2003

Abstract

The present study addresses a computational work of the weak shock wave propagating inside a silencer system of automobile exhaust pipe. The second order total variation diminishing (TVD) scheme is employed to solve the two-dimensional, compressible, unsteady, Euler equations. Eight different models of the silencer systems are explored to investigate the effects of the silencer configuration that has on the weak shock wave propagation phenomena. The incident plane shock wave is assumed at the inlet of the silencer and its Mach number is changed between 1.01 and 1.30. The present computational analysis clearly reveals the detailed shock wave reflections/diffractions and vortical flows inside the silencer models. These results are detailed by the pressure time histories at several locations inside the silencer model. Of the eight different silencers applied, the silencer model with a series of the baffle plates inside the expansion chamber reduces the first peak pressure at the exit of the exhaust pipe by about 27%. The present computational results predict the experimental results with a quite good accuracy.

1. Introduction

Flow-induced noise and vibration problems are often encountered in the pipelines conveying high-pressure gas or liquid. Unlike such problems occurring inside the pipelines, any other types of noises are generated when the high-pressure gas is discharged from the exit of a pipe system [1,2]. In usual, these noises have different features depending on whether the gas is discharged steadily and impulsively. An impulse noise is generated by a sudden discharge of gas flows from an exit of pipe [3,4]. For instance, the impulse noise is frequently found in

*Corresponding author. Tel.: +82-54-820-5622; fax: +82-54-823-1630.
E-mail address: kimhd@andong.ac.kr (H.-D. Kim).

0022-460X/$ - see front matter © 2003 Elsevier Ltd. All rights reserved.
doi:10.1016/j.jsv.2003.07.008

internal engine exhaust systems. Similar impulse noise problems are also found in a variety of unsteady flow devices, such as gun muzzles [5], high-speed railway tunnels [6,7], pulse jet applications [8,9], etc.

With a recent tendency of high noise emission internal engine, the impulse noise discharged from the exit of an engine exhaust pipe has been practically important issues from the point of view of silencer design. In the past, much effort has been paid on the silencer systems to reduce the flow-induced noise and vibration problems [10,11]. Almost all of the silencer systems have been designed based upon an assumption that the high-pressure gas flows steadily inside them.

Recently, several experimental works [12,13] showed that a weak shock wave, its Mach number being below about 1.1, can be formed inside the exhaust silencer system of internal combustion engine, when the engine is rotating at a high speed. The weak shock wave is generated due to a non-linear behavior of the compression waves discharged from the engine exhaust ports and it often leads to serious noise and vibration problems inside the exhaust pipe system.

Impulse wave [14,15] is generated as the shock wave is discharged from the exit of the exhaust pipe, causing unpleasant exhaust noises. Such an impulse wave is in general characterized by a sharp peak pressure of short duration [16]. The impulse noises generated from the engine exhaust pipe system have been one of the most important issues for automobile engine manufacturers to resolve urgently.

Sekine et al. [17,18] have made an experimental work to investigate the weak shock waves propagating inside the exhaust pipe system of a four-cycle gasoline engine. They have shown that a simple shock tube can simulate the shock wave propagation occurring in the automobile exhaust pipe system. They also have investigated several different types of silencer configurations appropriate to reduce the exhaust noises. Matsumura et al. [19] have used a shock tube to find the optimum silencer configuration against the engine exhaust noises. From these experimental works, the data needed to practically design the silencer systems are not sufficient due to some limits in the experimental measurements.

A computational work can provide useful and practical data for the silencer design, but, to the authors' knowledge, there are to date no any computational works made on this topics. Thus, more experimental and computational studies are necessary to clarify the characteristics of the exhaust pipe systems and to obtain the optimum silencer configuration.

The present study addresses a computational work to investigate detailed characteristics of the weak shock wave propagating through an exhaust pipe silencer system. The unsteady, two-dimensional, inviscid, compressible, Euler equations were numerically solved using Yee–Rod–Davis's total variation diminishing (TVD) scheme, and the computational results were compared with the previous experiments [20] for the purpose of validation. In computations, a plane shock wave was assumed at the inlet of the exhaust pipe and its Mach number M_s was changed in the range from 1.01 to 1.30. In order to investigate the effect of the silencer configuration on the reduction of the exhaust noises, eight different types of silencers were applied to the present computations. The results obtained showed that of these silencers, the silencer model with a series of baffle plates in an expansion chamber reduced the peak pressure at the exit of the exhaust pipe by about 27%, compared with that at the base model of the simplified expansion chamber.

2. Computational analysis

2.1. Governing equations

In order to simulate the weak shock wave propagating through an exhaust pipe silencer system, the two-dimensional, unsteady, compressible, Euler equations are employed in the present study. The governing conservation equations are given by

$$\frac{\partial U}{\partial t}+\frac{\partial F}{\partial x}+\frac{\partial G}{\partial y}=0, \tag{1}$$

where

$$U=\begin{bmatrix}\rho\\ \rho u\\ \rho v\\ e\end{bmatrix},\ F=\begin{bmatrix}\rho u\\ \rho u^2+p\\ \rho uv\\ (e+p)u\end{bmatrix},\ G=\begin{bmatrix}\rho v\\ \rho uv\\ \rho v^2+p\\ (e+p)v\end{bmatrix}$$

and x is the longitudinal distance, y is the transverse distance, ρ is the density and u and v are the velocity components for the x and y directions, respectively. The total energy, e per unit volume of the gas is expressed by the sum of the kinetic energy and the internal energy as follows:

$$e=\frac{p}{\gamma-1}+\rho\left(\frac{u^2+v^2}{2}\right). \tag{2}$$

Eq. (1) is closed by the thermal equation of the state of a perfect gas, $p=\rho RT$, where T is the temperature. In computations, Eq. (1) is rewritten in a non-dimensional form by referring the quantities, the pressure, the density, etc., at atmospheric conditions and the diameter of the shock tube, as next;

$$p'=\frac{p}{p_1},\quad \rho'=\frac{\rho}{\rho_1},\quad u'=\frac{u}{a_1/\sqrt{\gamma}},\quad v'=\frac{v}{a_1/\sqrt{\gamma}},$$
$$t'=\frac{t}{(D/a_1)\sqrt{\gamma}},\quad x'=\frac{x}{D},\quad y'=\frac{y}{D}, \tag{3}$$

where subscripts 1 indicates the atmospheric condition, D the diameter of shock tube and a_1 the speed of sound under the atmospheric condition. The symbol ($'$), indicating the non-dimensional quantities, is omitted for the sake of simplicity and then the equation system is just the same formula to Eq. (1).

2.2. Numerical scheme

TVD scheme have proven to be very effective for computing the phenomena of shock waves without presenting the spurious oscillations, which were associated with the conventional second order schemes in the presence of discontinuities. TVD scheme has made it possible to obtain non-oscillatory, but sharp approximations to shocks and contact discontinuities with higher than first order accuracy. The concept of the TVD scheme was first introduced by Harten [21], which guarantee that monotone profiles remain monotone.

The concept of bounded total variation finds its origin in an important property of a scalar conservation law $u_t + f_x = 0$: the total variation of any physically admissible solution $TV = \int |\partial u/\partial x| \mathrm{d}x$ does not increase in time. The total variation in x (TVD) of a discrete solution to a scalar conservation law is defined by

$$TV(u) \equiv \sum_i [u_{i+1} - u_i]. \tag{4}$$

A numerical solution is said to be of bounded total variation or total variation stable if the total variation is uniformly bounded in t and Δx. To allow for higher accuracy, Harten proposed the TVD condition as the monotonicity condition to be satisfied by the scheme:

$$TV(u^{n+1}) \leqslant TV(u^n). \tag{5}$$

A scheme satisfying the above condition is called a TVD scheme. After the introduction of TVD scheme by Harten, the TVD scheme was further modified by Yee, Davis, Roe, etc.

For the present computational analysis, the Yee–Roe–Davis's TVD scheme [22] is applied to discretize the governing equations. For computation of the time-dependent flows, an operator splitting technique, which was suggested by Sod [23] is employed for temporal and spatial derivatives, and then Eq. (1) can be given by a set of one-dimensional equations

$$L_x : \frac{\partial U}{\partial t} + \frac{\partial F}{\partial x} = 0, \; L_y : \frac{\partial U}{\partial t} + \frac{\partial G}{\partial y} = 0, \tag{6}$$

$$U_{i,j}^{n+2} = L_x L_y L_y L_x U_{i,j}^n, \tag{7}$$

$$L_x U_{i,j}^n = U_{i,j}^{n+1} = U_{i,j}^n - \frac{\Delta t}{\Delta x}[\hat{F}_{i+1/2}^n - \hat{F}_{i-1/2}^n], \tag{8}$$

where subscripts i,j, and superscript n indicate the space nodes and time step, and L_x, L_y the differential operators for the x direction and the y direction, respectively. In Eq. (8), Δt and Δx indicate the time interval and the grid space in the x direction, respectively, and $\hat{F}$ denotes the numerical flux in the x direction which is expressed as

$$\hat{F}_{i+1/2}^n = \tfrac{1}{2}[F_i^n + F_{i+1}^n + R_{i+1/2}^n \cdot \Phi_{i+1/2}^n], \tag{9}$$

where $R_{i+1/2}^n$ is a matrix whose column vectors are the right eigenvectors of the flux Jacobian $\partial F/\partial U$, evaluated with a symmetric average of $U_{i,j}$ and $U_{i+1,j}$. The last term $R_{i+1/2}^n \cdot \Phi_{i+1/2}^n$ represents the anti-diffusive flux contribution that corrects the excessive dissipation of first order numerical flux in a non-linear way. The numerical flux $\hat{G}_{j+1/2}^n$ in the y direction can be similarly expressed.

For Yee–Roe–Davis's second order symmetric TVD scheme, the vector $\Phi_{i+1/2}^n$ is given as

$$\Phi_{i+1/2} = -\left[\frac{\Delta t}{\Delta x}(a_{i+1/2})^2 g_{i+1/2} + \Psi(a_{i+1/2})(\alpha_{i+1/2} - g_{i+1/2})\right], \tag{10}$$

where $a_{i+1/2}$ is the eigenvalue of the flux Jacobian matrix in the x direction, $\alpha_{i+1/2}$ the forward difference of the local characteristic variables in the x direction, and $g_{i+1/2}$ the limiter function.

$\alpha_{i+1/2}$ and $g_{i+1/2}$ are defined as follows:

$$\alpha_{i+1/2} = R^{-1}_{i+1/2}(U_{i+1,j} - U_{i,j}), \tag{11}$$

$$g_{i+1/2} = \min \text{mod}(\alpha_{i-1/2},\ \alpha_{i+1/2},\ \alpha_{i+3/2}). \tag{12}$$

The function $\Psi(a_{i+1/2})$, called an entropy correction function, is defined as

$$\Psi(a_{i+1/2}) = \begin{cases} |a_{i+1/2}| & \text{if } |a_{i+1/2}| \geqslant \varepsilon, \\ (a^2_{i+1/2} + \varepsilon^2)/2\varepsilon & \text{if } |a_{i+1/2}| < \varepsilon, \end{cases} \tag{13}$$

where ε is a small positive number. This function corrects the entropy to prevent the entropy violating solutions, such as expansion shock waves.

2.3. Computational domain and boundary conditions

Fig. 1 schematically illustrates eight different models of the exhaust silencer system applied in the present computations, where d and D indicate the diameters of the exhaust pipe and silencer, respectively. For a comparison with the experiments carried out previously, the values of d and D are given by 20 and 80 mm, respectively. The silencer model 1 is a simplified silencer with an expansion chamber of a diameter of D. Its length is given by $10d$. In the present study, model 1 is used as a base model.

Model 2 is a double expansion chamber type, the length of each of the expansion chambers being $4d$. Model 3 has a horizontal plate inside the simple expansion chamber of the base model. Model 4 has the plates inserted from the upstream and downstream facing walls of the expansion chamber, and the plates are $2.5d$ and $5.0d$ long, respectively. The thickness of the plates is fixed at $0.5d$. In model 5, the length of the plates inserted from the upstream and downstream facing walls of the expansion chamber is the same to be $2.5d$. However, models 6 and 7 have the staggered plates inserted from the upstream and downstream facing walls of the expansion chamber. Finally, model 8 has a series of the baffle plates installed in the expansion chamber.

In order to characterize the shock waves propagating through the silencer models described above, the time-dependent pressures are obtained at the measuring points 1–4 (see the measuring points for each of the silencer models). The measuring points 1 and 4 correspond to the inlet and outlet of the silencer models, respectively, while the points 2 and 3 are inside the expansion chamber.

Fig. 2 shows the computational domain and boundary conditions for the silencer model 1, which is used as a base model. For the sake of the present computational analysis, the inlet of the expansion chamber is assumed to be an origin $x = 0$. The computational domain is extended to $-5d$ and $15d$, upstream and downstream of the expansion chamber, respectively. This domain was obtained by some preliminary tests for the computational domain effects on the obtained solutions. As an initial condition of computation, a plane incident shock wave of Mach number M_s is assumed at $x/d = -3.0$, and with a start of computation, it propagates toward the outlet of the silencer model. In the present study, the Mach number M_s of the incident shock wave is changed between 1.01 and 1.30, since the shock wave that appears inside the automobile exhaust pipe systems is, in practical, very weak.

As to the computational boundary conditions, the inflow and outflow conditions are applied to the upstream and downstream boundaries, respectively, which are expressed

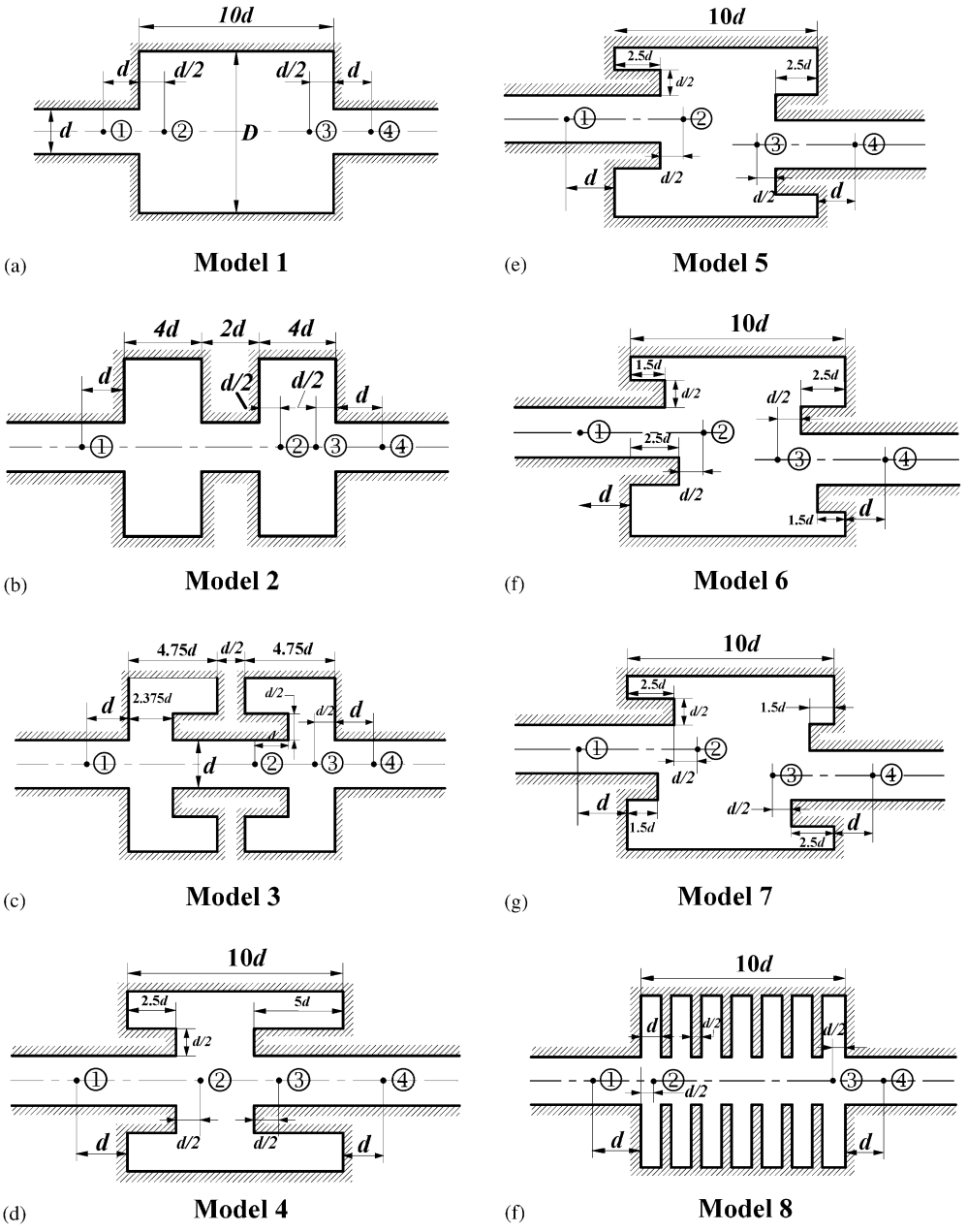

Fig. 1. Silencer models applied in computation.

as follows:

$$\begin{cases} \sigma_{n-1} = \sigma_{i+1}, \ \sigma_n = \sigma_i, & \text{inflow conditions,} \\ \sigma_i = \sigma_n = \sigma_{n+1}, & \text{outflow conditions,} \end{cases}$$

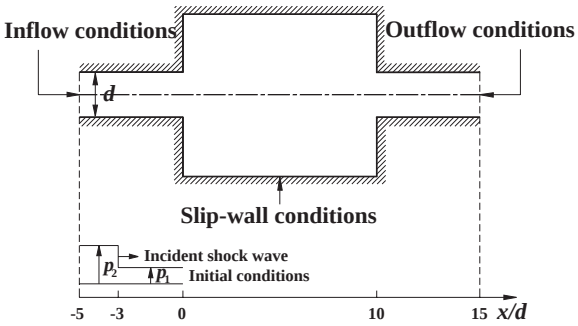

Fig. 2. Computational flow field and boundary conditions.

where σ is a quantity such as pressure, density, velocity, etc., and the subscripts i and n refer to the inner grid and the imaginary outer grid, respectively. The slip-wall conditions are applied to all of the solid walls. A square grid system is employed in the present computations.

The fineness of computational grid required to obtain grid independent solutions was first examined with the previous experimental data [20]. A grid density over $\Delta x = \Delta y = d/70$ seemed to no longer change the accuracy of the obtained solutions. A grid size of $\Delta x = \Delta y = d/75$ is employed so that the solutions obtained were independent of the grid density. The grid numbers of about 450,000 are used in the present computations.

3. Results and discussion

Fig. 3 shows the propagation processes of the weak shock wave inside the silencer model 1, where the Mach number M_s of the incident shock wave is 1.1, and time t is assumed to be zero as the incident shock wave locates at $x/d = -3.0$. From the present computations, it is found that at $t = 0.56$ ms, the normal shock wave locates just upstream of the expansion chamber. At $t = 0.67$ ms, the shock wave propagates into the expansion chamber and the resulting wave patterns are curved. It is found that the curved shock wave has the regular reflections on the upper and lower walls of the expansion chamber, and the strong vortical flows are formed at the inlet of the expansion chamber. At $t = 0.77$ ms, the strong interactions between the reflected shock waves and the vortical flows are found around the inlet of the expansion chamber. With time, the curved shock wave propagates toward the outlet of the expansion chamber, and in this case, the Mach reflections are found on the upper and lower walls of the expansion chamber. At $t = 1.03$ ms, it seems that the curved shock wave becomes nearly normal to the axis of the silencer. With time, a part of the shock wave propagates into the exhaust pipe downstream of the expansion chamber, the resulting shock wave being normal and quite weak in the exhaust pipe, while the other part of the shock wave is reflected back from the outlet of the expansion chamber. Very complicated wave structures are found around the outlet of the expansion chamber. From a comparison between the present computations and experiments [20], it is found that the present computations predict the experimented flow fields with a quite good accuracy.

Fig. 4 shows the pressure time histories at the measuring points 1–4 in the silencer model 1, where $M_s = 1.1$ and $D/d = 4.0$. The solid and broken lines present the present computational

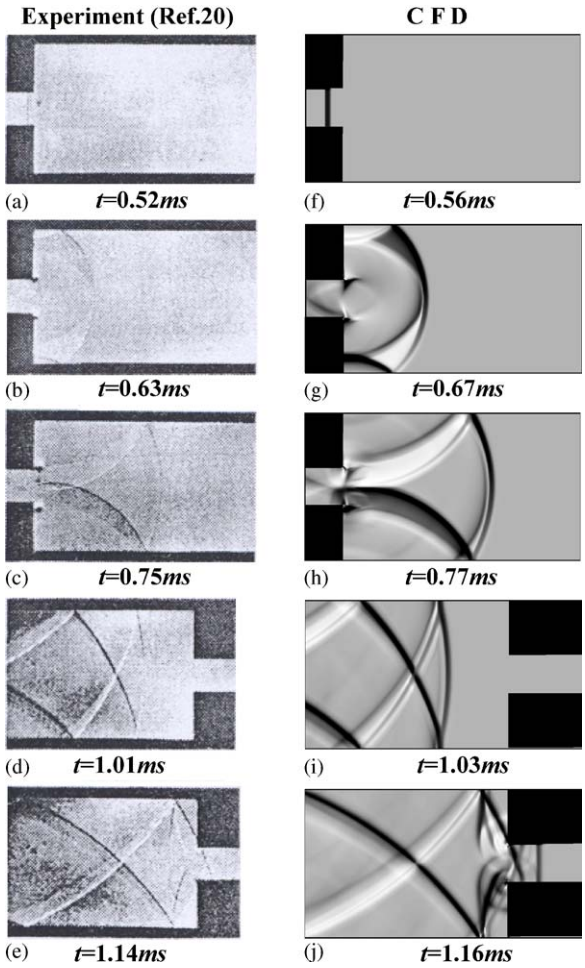

Fig. 3. Experimented and computed Schlieren images for silencer model 1 ($M_s = 1.1, D/d = 4.0$).

results and experiments [20], respectively. At the measuring point 1 in the exhaust pipe upstream of the expansion chamber, the pressure sharply rises up to certain over pressure level, as the incident shock wave reaches the measuring point, and it remains constant for a short time. Then the pressure suddenly decreases, as the expansion waves propagate back from the inlet of the expansion chamber. The pressure rises again due to the effects of the shock waves reflected from the upper and lower walls of the expansion chamber. At $t = 1.80$ ms, the pressure rise is due to the shock wave reflected back from the upstream facing wall of the expansion chamber.

At the measuring point 2 inside the expansion chamber, the pressure sharply rises to a certain peak value due to the shock wave propagating into the expansion chamber. A sharp peak pressure of short duration is formed at the measuring point 2. Then the pressure fluctuates with time due to the repeated wave reflections inside the silencer system. At $t = 1.7$ ms, the pressure rises again due to the shock wave reflected back from the upstream facing wall of the expansion chamber. At the measuring points 3 and 4, the pressure rise seems rather gradual, compared with that at the

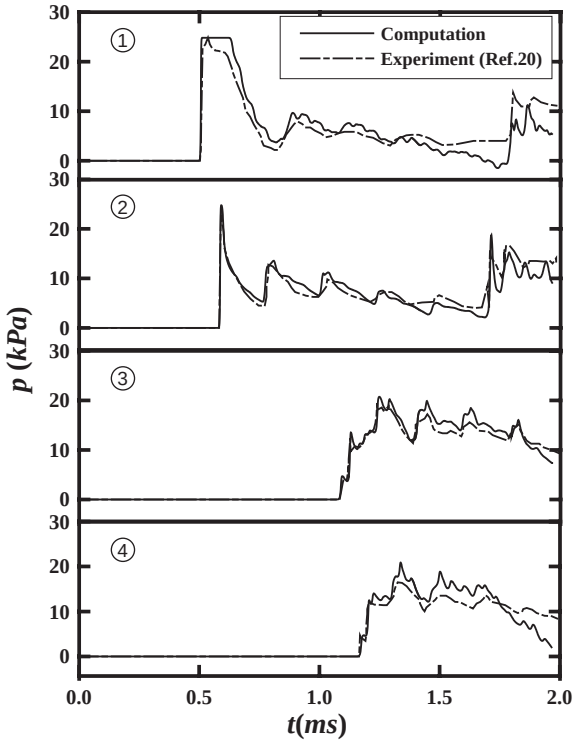

Fig. 4. Pressure variations at various measuring points for silencer model 1 ($M_s = 1.1, D/d = 4.0$).

measuring point 2, and the peak over pressure level is considerably lower than that of the measuring point 2. It is found that the present computation well predicts the experimented pressure time histories.

For the silencer model 2, which has double expansion chamber, Fig. 5 shows a comparison between the predicted and experimented wave patterns inside the silencer system. At $t = 0.52$ ms, the incident shock wave locates inside the exhaust pipe upstream of the expansion chamber. At $t = 0.62$ ms, the shock wave propagates into the first expansion chamber, resulting in a curved wave, and the reflected waves propagate back toward the exhaust pipe upstream of the expansion chamber. The vortical flows are formed at the inlet of the expansion chamber. At $t = 0.81$ ms, a part of the shock wave propagates into the second expansion chamber, while the other part of the shock wave reflects back from the upstream facing wall of the first expansion chamber. At the inlet of the first expansion chamber, the vortical flows develop with time and those are also generated at the inlet of the second expansion chamber, but their strength seems somewhat weaker, compared with those at the inlet of the first expansion chamber. At $t = 0.89$ ms, the shock wave propagates toward the outlet of the second expansion chamber, and then it goes through the exhaust pipe downstream of the second expansion chamber, as a weak normal shock wave with a reduced magnitude.

The flow fields inside the silencer model 2 are more detailed by the pressure time histories, as shown in Fig. 6. At the measuring point 1, the pressure sharply rises as the initial shock wave

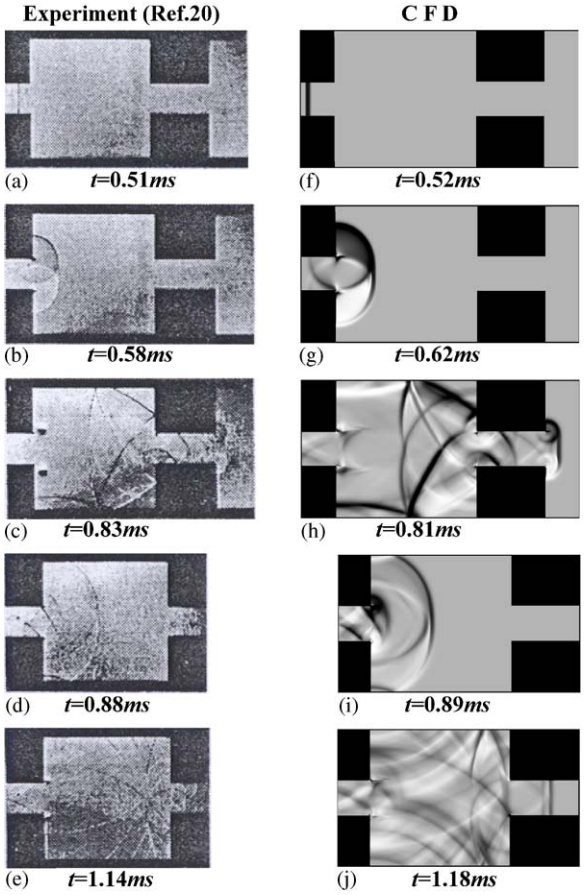

Fig. 5. Experimented and computed Schlieren images for silencer model 2 ($M_s = 1.1, D/d = 4.0$).

reaches the measuring point and it remains constant for a short time before the expansion waves are reflected back from the downstream facing wall of the first expansion chamber. At $t = 0.83$ ms, the pressure increases due to the effect of the reflected shock wave from the first expansion chamber. A sharp pressure increase is found again at $t = 1.16$ ms. This is due to the shock wave reflected back from the upstream facing wall of the first expansion chamber. At the measuring points 2, 3, and 4, the several peaks are found in the pressure time histories. Of them, the first peak is made by the incident normal shock wave. It is interesting to note that at the measuring point 2, the first peak seems to be considerably lower than that at the measuring point 1 and, moreover, at the measuring point 4 it is much lower than that at the measuring point 2.

From a comparison between the predicted and experimented pressure histories obtained at the measuring point 1 the present computation well predicts the experimented pressure histories for $t < 1.5$ ms, but a discrepancy between both the pressure histories is quite large for $t > 1.5$ ms. Furthermore, the present computations fail in predicting the peak pressures at the measuring points 2, 3 and 4 although it seems that the present computation predicts the first peak pressure with a good accuracy. These discrepancies can be, in part, due to the viscous effects that are

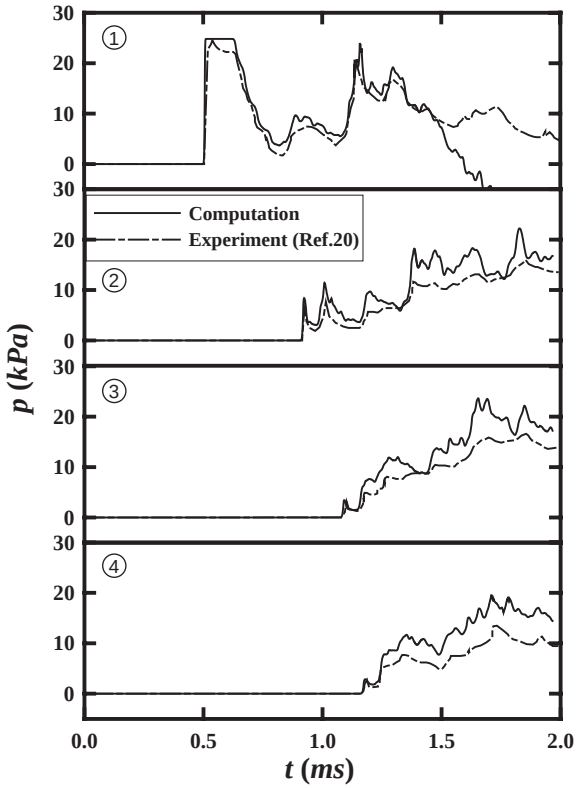

Fig. 6. Pressure variations at various measuring points for silencer model 2 ($M_s = 1.1, D/d = 4.0$).

ignored in the present study. Thus a better prediction may be obtained by the computation involving the viscous and thermal effects.

Fig. 7 shows the computed and experimented Schlieren images of the shock waves in the silencer model 3. The incident shock wave propagates into the expansion chamber, and strong wave diffractions and reflections appear around the horizontal plates inside the expansion chamber. These can reduce the magnitude of the shock wave propagating into the exhaust pipe downstream of the expansion chamber, as observed at $t = 1.18$ ms. The present computation predicts the experimented wave structures with a quite good accuracy. Fig. 8 shows the predicted and experimented pressure time histories. The present computation well predicts the first peak pressure, which is caused by the incident shock wave, but again fails in predicting the pressure fluctuations behind the first peak pressure.

Fig. 9 shows the computed and experimented Schlieren images of the shock waves in the silencer model 4, which has the inserted plates inside the expansion chamber. It is interesting to note that the incident shock wave propagating inside the pipe is faster than that inside the expansion chamber, as observed at $t = 1.89$ ms. This is due to the flow passage area effect on the velocity of the shock wave propagation. The computed results well predict the complicated wave phenomena inside the silencer model 4. Fig. 10 shows the predicted and experimented pressure time histories. At the measuring point 1 the present computation predicts the constant

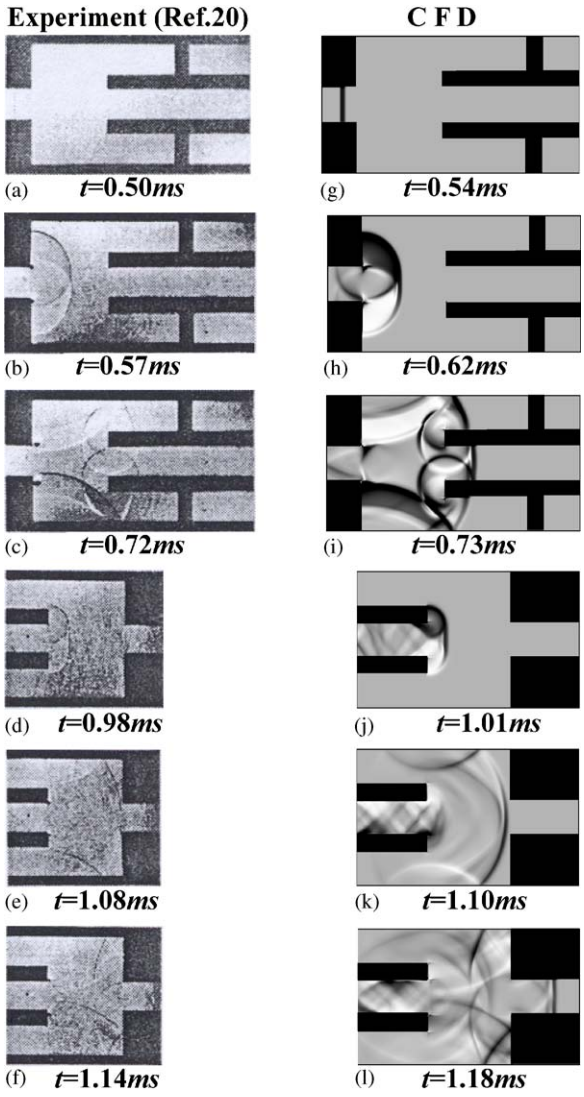

Fig. 7. Experimented and computed Schlieren images for silencer model 3 ($M_s = 1.1, D/d = 4.0$).

peak pressure level just behind the incident shock wave, while the experimented result indicates the pressure gradually decreasing with time just behind the incident shock wave. In the experiment, it should be noted that a series of baffle plates were inserted into the high pressure chamber of the shock tube in order to make a certain pulse-like pressure wave inside the low pressure chamber. The present computation satisfactorily predicts the first peak pressure and the pressures just behind the incident shock wave as well.

Figs. 11–14 show the predicted Schlieren images of the shock waves in the silencer models 5–8, respectively. For the silencer models 5–7, the shock wave propagations and diffractions appear asymmetric, since, in these cases, the silencer configurations are asymmetric against the pipe axis.

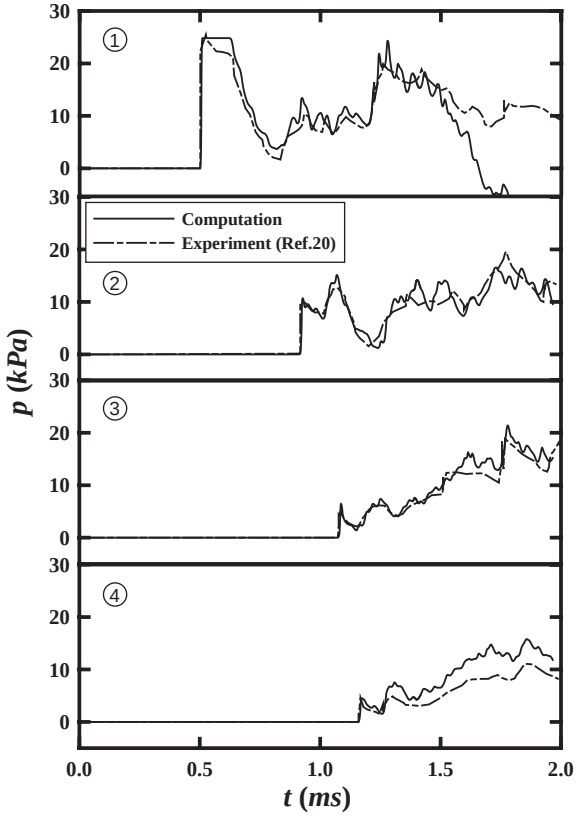

Fig. 8. Pressure variations at various measuring points for silencer model 3 ($M_s = 1.1, D/d = 4.0$).

Thus the transmitted shock wave inside the pipe, downstream of the expansion chamber, appears somewhat oblique. Compared with the symmetric silencer configurations that were described previously, the wave reflections and diffractions seem to be more complicated inside the expansion chamber.

Fig. 14 shows the predicted Schlieren images of the weak shock waves in the silencer model 8 which has a series of baffle plates inside the expansion chamber. Very complicated wave reflections and diffractions are observed between the baffle plates, the waves being quite symmetric. At $t = 1.16$ ms, a weak normal shock wave which propagates through the baffle plates inside the expansion chamber is found in the outlet of the pipe. Strong wave reflections and diffractions, which are generated upstream inside the expansion chamber, seem to considerably attenuate downstream.

Fig. 15 represents the predicted pressure time histories, corresponding to the flow conditions described in Figs. 11–14. At each of the measuring points, the pressures highly fluctuate with time. A constant peak pressure level, which is made by the incident shock wave, is found for the silencer model 5, and its duration seems to be longer, compared with the other models. This is due to the expansion waves propagating back toward the inlet of the pipe. The first peak pressures obtained at the measuring points 2, 3, and 4 can be compared with each other for each of the silencer

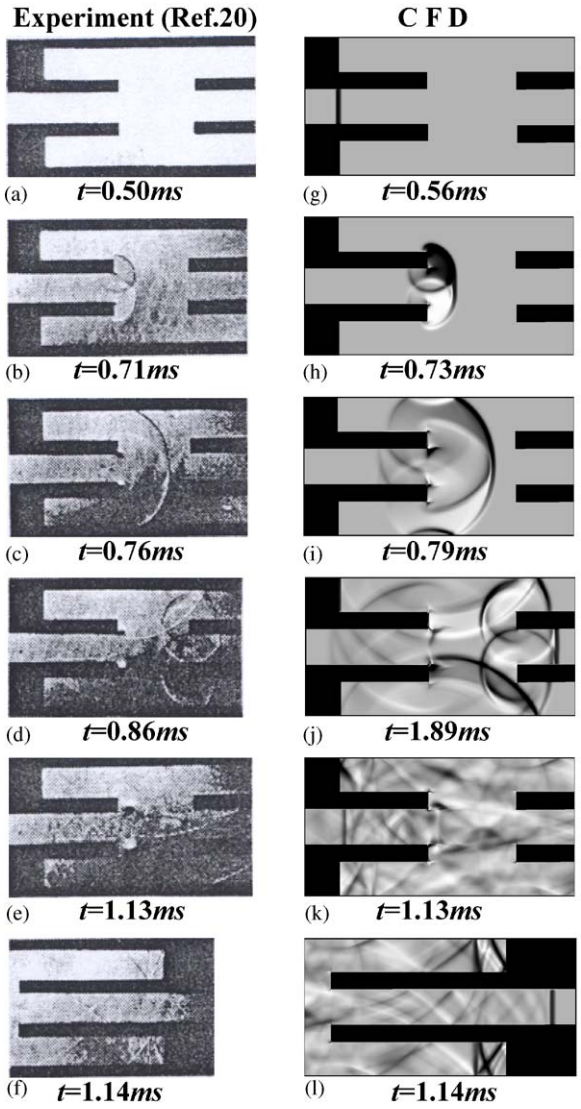

Fig. 9. Experimented and computed Schlieren images for silencer model 4 ($M_s = 1.1, D/d = 4.0$).

models. It is worthwhile noting that at the measuring point 4, the first peak of the pressure time histories, which is caused by the incident shock wave, is lowest in model 8, but at $t = 1.8$ ms a high second peak is also found in this model. The first peak pressure and its time-gradient are associated with the impulse wave discharged from the exit of the engine exhaust pipe [16]. Each of the silencer models, applied in the present study, shows different pressure time histories at the exit of the pipe. This fact implies that an optimal configuration for an automobile exhaust silence system can be obtained in the models mentioned above.

In order to compare the first peak pressures in all the silencer models, Fig. 16 represents the pressure time histories at the measuring point 4, corresponding to the exit of the exhaust pipe. All

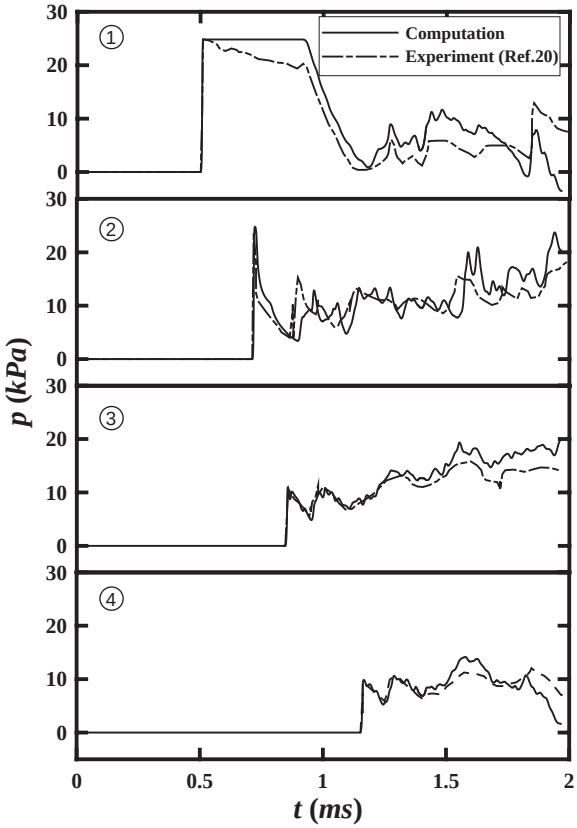

Fig. 10. Pressure variations at various measuring points for silencer model 4 ($M_s = 1.1, D/d = 4.0$).

the flow conditions are the same for the eight silencer models, where $M_s = 1.1$ and $D/d = 4.0$. It is found that the first peak pressure is the smallest in model 8, while it is the highest in model 4. It seems that models 4–7 produce the first peak pressure higher than that in the base model 1, while models 2, 3 and 8 produces the first peak pressure peak lower than the base model 1. Meanwhile, the pressures behind the first peak pressure highly fluctuate with time, strongly depending on the silencer models. It is difficult to compare the peak pressures produced after the first peak pressure. This is because those are resulted from very complicated wave phenomena inside the expansion chamber and have very different pressure histories and durations.

Fig. 17 shows the decay ratio of the first peak over-pressure for various Mach numbers of the incident shock wave M_s, where p_{in} and p_{out} indicate the over-pressure made by the initial shock wave at the measuring point 1 and the first peak over-pressure by the transmitted shock wave at the measuring point 4, respectively. The solid lines present the present computational results. For a given M_s, all the silencer models significantly attenuate p_{out}/p_{in} values, compared with no silencer model of a straight exhaust pipe. It seems that model 8 is the most effective to reduce the first peak over pressure. The Mach number M_s of the incident shock wave in the silencer model 8 negligibly affects the decay ratio of the first peak over-pressure p_{out}/p_{in}, but in the other models,

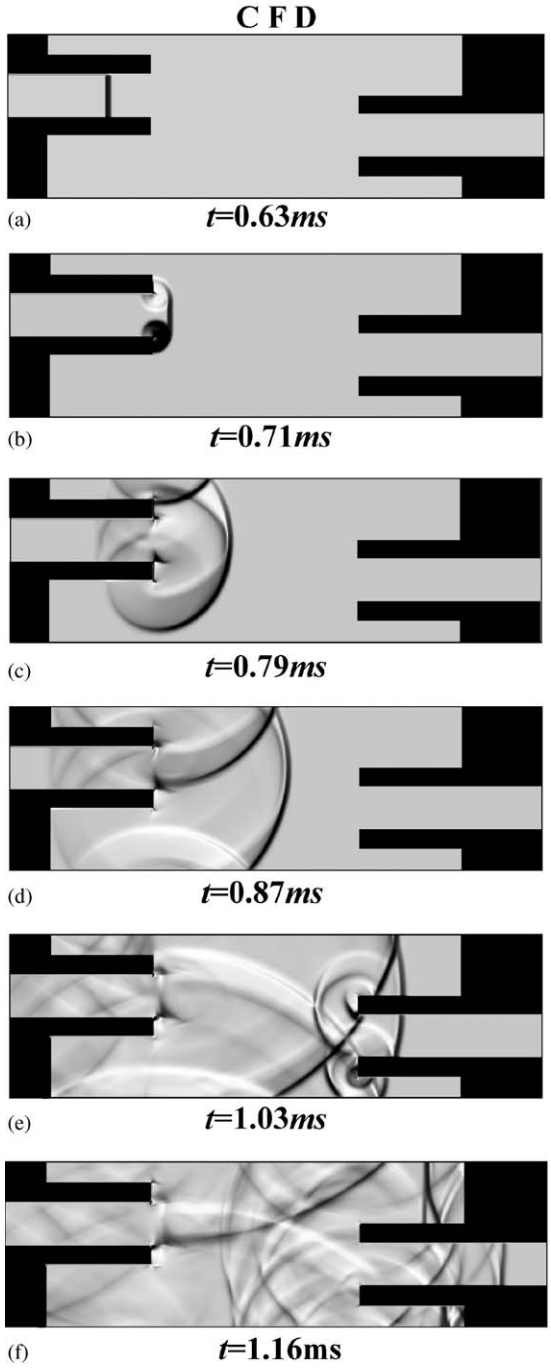

Fig. 11. Computed Schlieren images for silencer model 5 ($M_s = 1.1, D/d = 4.0$).

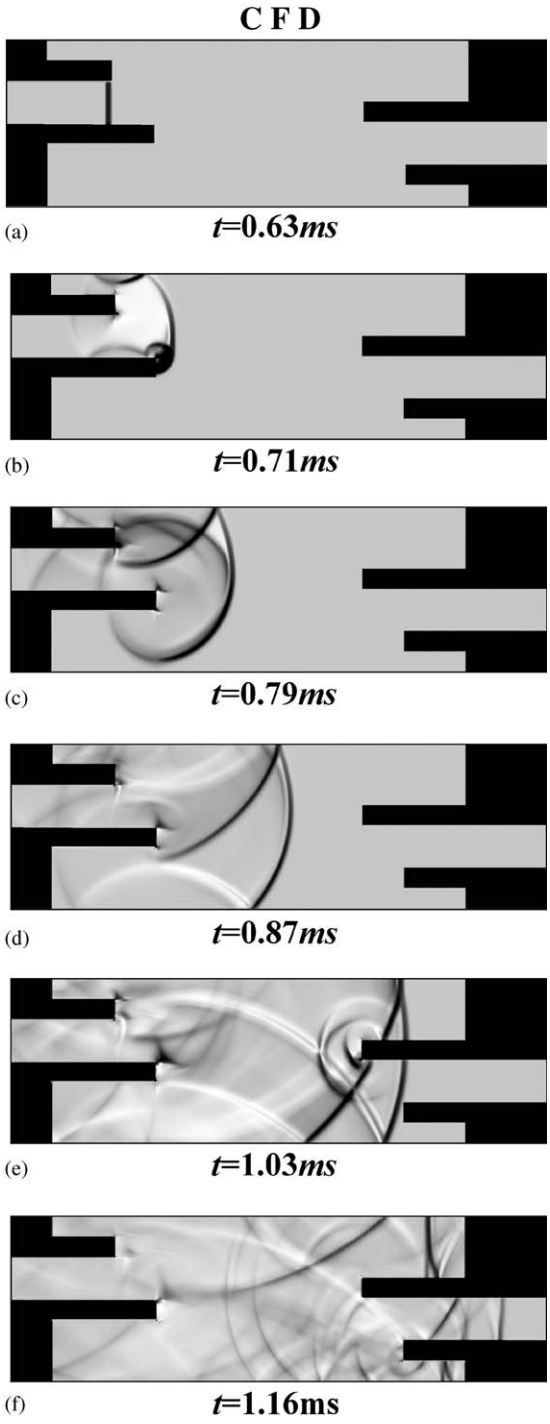

Fig. 12. Computed Schlieren images for silencer model 6 ($M_s = 1.1, D/d = 4.0$).

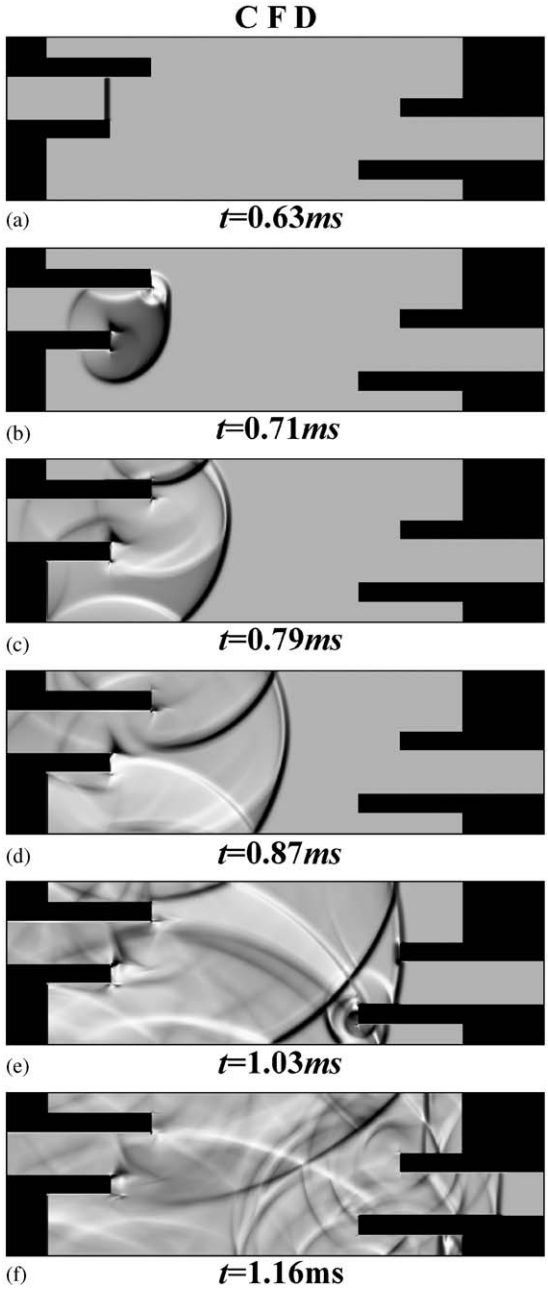

Fig. 13. Computed Schlieren images for silencer model 7 ($M_s = 1.1, D/d = 4.0$).

the decay ratio is a weak function of the Mach number; p_{out}/p_{in} somewhat decreases with an increase in M_s. This is due to the fact that the higher the Mach number of the incident shock wave, the stronger are the shock wave reflections and diffractions inside the expansion chamber.

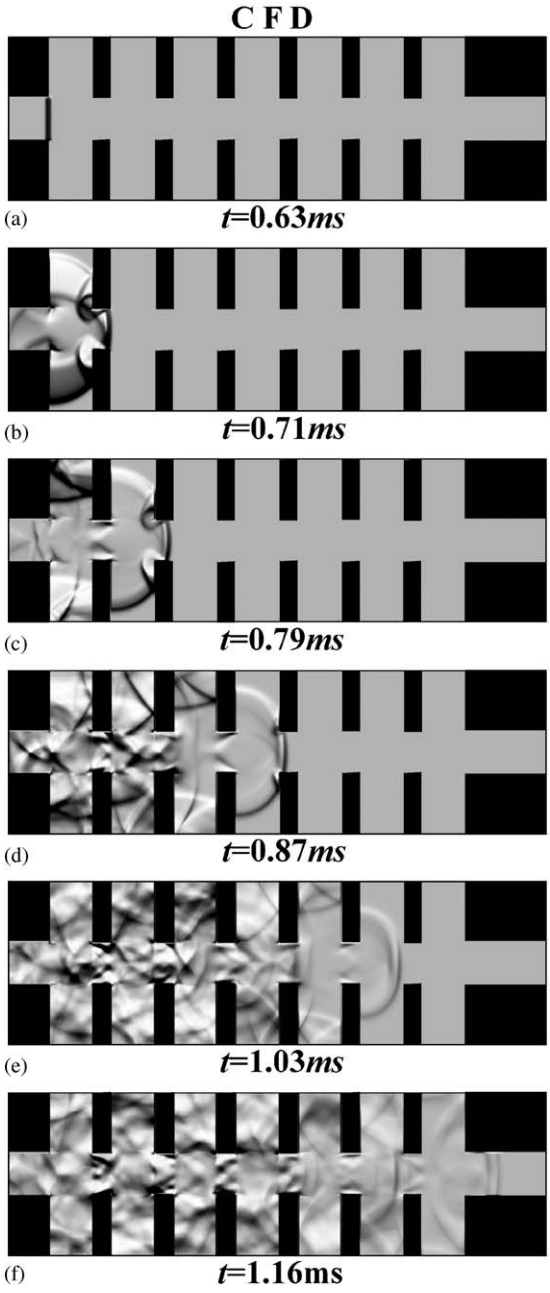

Fig. 14. Computed Schlieren images for silencer model 8 ($M_s = 1.1, D/d = 4.0$).

4. Conclusions

The present study describes a computational work to investigate detailed characteristics of the weak shock wave propagating through an engine exhaust silencer system. Computational analysis

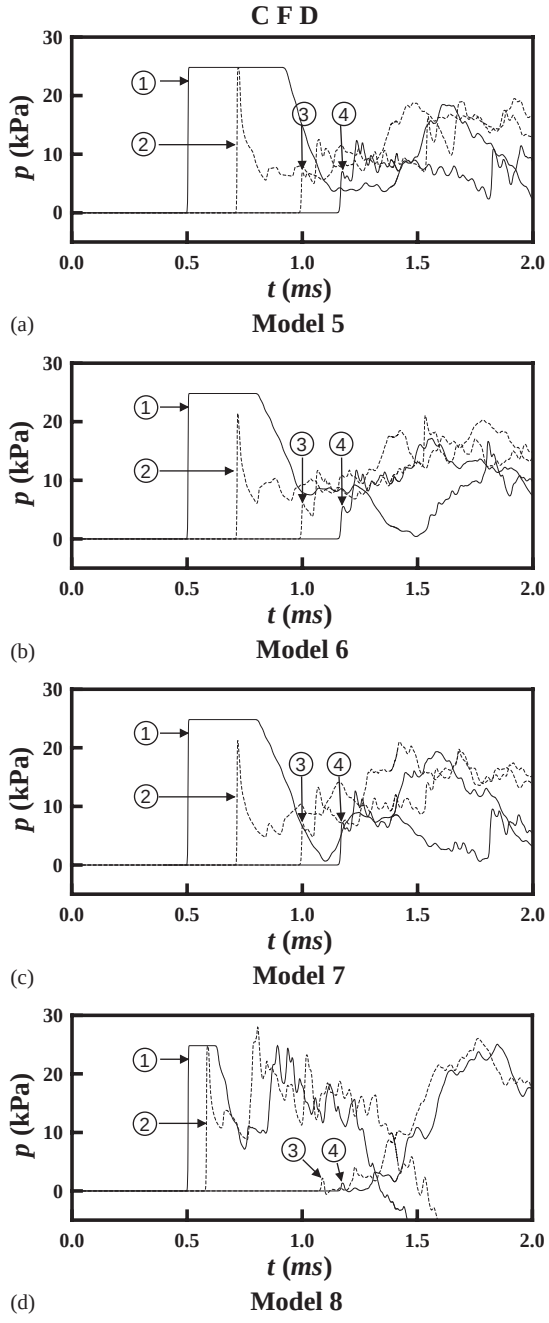

Fig. 15. Predicted pressure variations at various measuring points for silencer models 5, 6, 7 and 8 ($M_s = 1.1, D/d = 4.0$).

was applied to simulate the experimental flow fields, subject to the unsteady, two-dimensional, inviscid, compressible, Euler equations, using a TVD scheme. Eight different models of the silencer systems were tested to investigate the effects of the silencer configuration that has on

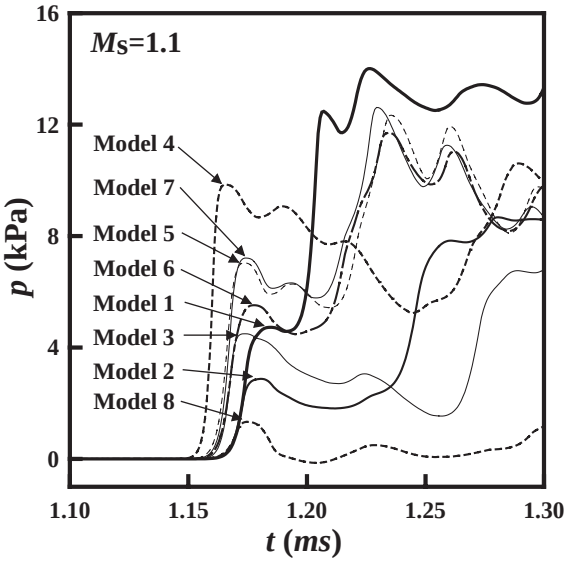

Fig. 16. Pressure variations at measuring points ④ for various silencer models ($M_s = 1.1, D/d = 4.0$).

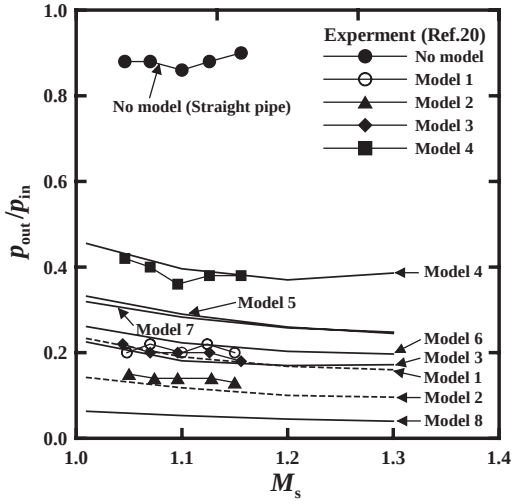

Fig. 17. Decay ratio of the first peak over-pressures.

the weak shock wave propagation phenomena. The incident plane shock wave was assumed at the inlet of the silencer and its Mach number was changed between 1.01 and 1.30. The present computational analysis clearly showed the detailed shock wave reflections/diffractions and vortical flows inside the silencer models. These results were detailed by the pressure time histories at several locations inside the silencer model. From the pressure time history obtained at the outlet of the silencer, the first peak pressures were compared with each other for each of the silencer

models employed. Of the eight different silencers applied, the silencer model with a series of the baffle plates inside the expansion chamber reduced the first peak pressure at the exit of the exhaust pipe by about 27%. The present computational results predict the experimental results with a quite good accuracy.

Appendix A. Nomenclature

a	speed of sound, eigenvalue of flux Jacobian matrix
e	total energy per unit volume
M	Mach number
p	static pressure
t	time
u	velocity component in the x direction
v	velocity component in the y direction
x	longitudinal distance in Cartesian co-ordinate
y	transverse distance in Cartesian co-ordinate
γ	ratio of specific heats
ρ	density
d	diameter of pipe
D	diameter of silencer
L	differential operator
Δt	time interval
Δx	grid space in the x direction
F	numerical flux in the x direction
R	right eigenvector of the flux Jacobian
g	limiter function
ψ	entropy correction function

Sub/superscripts

1	atmosphere state
2	state behind the incident shock wave
$'$	non-dimensional quantity
n	time step
s	incident shock wave
i	space node in the x direction
j	space node in the y direction
in	pipe inlet
out	pipe outlet

References

[1] J.K. Floyd, Control of stream venting noise in power plants, *Transactions of the American Society of Mechanical Engineers, Journal of Engineering for Power* 100 (1978) 369–373.

[2] D.Y. Maa, P. Li, Pressure dependence of jet noise and silencing of blow-offs, *Noise Control Engineering* 17 (3) (1981) 104–112.
[3] H.D. Kim, T. Setoguchi, Study of the discharge of weak shocks from an open end of a duct, *Journal of Sound and Vibration* 226 (5) (1999) 1101–1128.
[4] P. Li, G. Dai, Z. Zhu, Noise radiation of a strongly pulsating tailpipe exhaust, *Journal of Sound and Vibration* 167 (3) (1993) 385–400.
[5] G. Klingenberg, J.M. Heimerl, Gun muzzle blast and flash, Progress in Astronautics and Aeronautics, American Institute of Aeronautics and Astronautics, Educational Series, 1992.
[6] R.S. Raghunathan, H.D. Kim, T. Setoguchi, Aerodynamic of high-speed railway train, *Progress in Aerospace Sciences* 38 (2002) 469–514.
[7] M. Bellenoue, V. Moriniere, T. Kageyama, Experimental 3-D simulation of the compression wave, due to train tunnel entry, *Journal of Fluids and Structures* 16 (5) (2002) 581–595.
[8] R. Klingel, F. Loffler, Dust collection and cleaning efficiency of a pulse jet fabric filters, *Proceedings of Filtration Society, Filtration and Separation* 20 (1983) 205.
[9] W.J. Morris, Cleaning mechanism in pulse jet fabric filters, *Proceedings of Filtration Society, Filtration and Separation* 21 (1984) 52.
[10] Y.H. Kim, J.W. Choi, B.D. Lim, Acoustic characteristic of an expansion chamber with constant mass flow and steady temperature gradient (theory and simulation), *Transactions of American Society of Mechanical Engineering* 112 (1990) 460–467.
[11] A.J. Green, P.N. Smith, Gas flow noise and pressure loss in heavy vehicle exhaust systems, *IMechE* C17/18 (1988) 47–54.
[12] A. Selamet, V. Kothamasu, J.M. Novak, R.A. Kach, Experimental investigation of in-duct insertion loss of catalysts in internal combustion engines, *Applied Acoustics* 60 (2000) 451–487.
[13] P.O.A.L. Davies, K.R. Holland, The observed aeroacoustic behaviour of some flow-excited expansion chambers, *Journal of Sound and Vibration* 239 (4) (2001) 695–708.
[14] H.D. Kim, D.H. Lee, T. Setoguchi, Study of the impulse wave discharged from the exit of a right-angle pipe bend, *Journal of Sound and Vibration* 259 (5) (2003) 1147–1161.
[15] H.D. Kim, T. Setoguchi, H. Kashimura, R.S. Raghunathan, Augmentation of the magnitude of the impulsive wave discharging from a tube, *IMechE Part C* 215 (2001) 191–199.
[16] R.S. Raghunathan, H.D. Kim, T. Setoguchi, Impulse noise and its control, *Progress in Aerospace Science* 34 (1) (1998) 1–44.
[17] N. Sekine, S. Matsumura, K. Aoki, K. Takayama, Generation and propagation of shock waves in the exhaust pipe of a four cycle automobile engine, in: *Proceedings of the 17th International Symposium on Shock Wave and Shock Tubes*, 1989, pp. 671–676.
[18] N. Sekine, I. Kudo, O. Onodera, K. Takayama, Effects of shock waves on silencer characteristics in the exhaust gas flow of automobile engines, *Shock Waves @ Marseille* III, 1995, pp. 359–366.
[19] S. Matsumura, O. Onodera, K. Takayama, Noise induced by weak shock waves in automobile exhaust systems (effects of viscosity and back pressure), *Shock Waves @ Marseille* III, 1995, pp. 367–372.
[20] I. Sakamoto, F. Higashino, K. Higuchi, Decay of pressure waves passing through expansion region in a two dimensional duct (in Japanese), *Japan Society of Mechanical Engineers, Journal Series B* 67 (657) (2001) 1170–1176.
[21] A. Harten, A high resolution scheme for the computation of weak solutions of hyperbolic conservation laws, *Journal of Computational Physics* 49 (1983) 357–393.
[22] H.C. Yee, Upwind and symmetric shock capturing schemes, NASA TM-89464, 1987.
[23] G.A. Sod, A numerical study of a converging cylindrical shock, *Journal of Fluid Mechanics* 83 (1977) 785–794.